LES of the convective boundary layer: A minimum-dissipation modeling approach

By M. Abkar AND P. Moin

1. Motivation and objectives

Large-eddy simulation (LES) is an important tool for studying the atmospheric boundary layer (ABL) (Deardorff 1974; Moeng 1984; Nieuwstadt *et al.* 1993; Mason 1994; Kosovic 1997; Porté-Agel *et al.* 2000; Bou-Zeid *et al.* 2005; Beare *et al.* 2006; Sullivan & Patton 2011; Zhou & Chow 2011). In LES, turbulent structures larger than a filter scale are resolved, and a subfilter model is used to account for the contribution of the unresolved small scales. Applying a spatial filter to the Navier-Stokes equations (here, including buoyancy and Coriolis effects) as well as the transport equation for the potential temperature leads to

$$\partial_i \tilde{u}_i = 0,\ \partial_t \tilde{u}_i + \partial_j(\tilde{u}_i\tilde{u}_j) = -\partial_i \tilde{p} + \partial_j(\nu\partial_j\tilde{u}_i) - \partial_j\tau_{ij} + \delta_{i3}\beta(\tilde{\theta} - \langle\tilde{\theta}\rangle) + f_c\varepsilon_{ij3}\tilde{u}_j,$$

$$\partial_t\tilde{\theta} + \partial_i(\tilde{u}_i\tilde{\theta}) = \partial_i(D\partial_i\tilde{\theta}) - \partial_i q_i, \tag{1.1}$$

where the tilde represents a spatial filtering; $\tilde{u}_i$ is the resolved velocity in the i-direction (with $i = 1, 2, 3$ corresponding to the streamwise (x), spanwise (y), and wall-normal (z) directions, respectively); $\tilde{\theta}$ denotes the resolved potential temperature; $\tilde{p}$ is the kinematic pressure; ν and D are the molecular viscosity and diffusivity, respectively; f_c is the Coriolis parameter; and ε_{ijk} is the alternating unit tensor. $\tau_{ij} = \widetilde{u_iu_j} - \tilde{u}_i\tilde{u}_j$ is the subfilter stress tensor, and $q_i = \widetilde{u_i\theta} - \tilde{u}_i\tilde{\theta}$ is the subfilter heat flux. In the momentum conservation equation, the buoyancy effects are accounted for via the Boussinesq approximation, in which $\beta = g/\theta_0$ is the buoyancy parameter, g is the gravitational acceleration, θ_0 is the reference potential temperature, δ_{ij} is the Kronecker delta tensor, and the angle brackets denote a horizontal average (Deardorff 1974).

An important class of subfilter models consists of eddy-viscosity/eddy-diffusivity models. These models incorporate the effect of unresolved eddies by locally increasing the molecular viscosity/diffusivity using an eddy viscosity/eddy diffusivity. In this approach, the subfilter turbulent fluxes are evaluated as

$$\tau_{ij}^d = \tau_{ij} - \frac{1}{3}\delta_{ij}\tau_{kk} = -2\nu_e\tilde{S}_{ij}, \quad q_i = -D_e\partial_i\tilde{\theta}, \tag{1.2}$$

where $\tilde{S}_{ij} = (\partial_i\tilde{u}_j + \partial_j\tilde{u}_i)/2$ is the resolved strain-rate tensor, ν_e is the eddy viscosity, and D_e is the eddy diffusivity. D_e is related to ν_e by the subfilter Prandtl number Pr_e, such that $D_e = \nu_e Pr_e^{-1}$. A popular way of modeling the eddy viscosity is to use the mixing length approximation, which yields the well-known Smagorinsky model (Smagorinsky 1963). In this approach, the eddy viscosity is modeled as $\nu_e = (C_s\Delta)^2|\tilde{S}|$, where $|\tilde{S}| = \sqrt{2\tilde{S}_{ij}\tilde{S}_{ij}}$ and C_s is the Smagorinsky coefficient. In a similar way, the subfilter eddy diffusivity is modeled as $D_e = \Delta^2 C_s^2 Pr_e^{-1}|\tilde{S}|$, where $C_s^2 Pr_e^{-1}$ is a lumped coefficient. One of the main challenges in the implementation of eddy-viscosity/eddy-diffusivity models is the specification of the model coefficients. In traditional LES of

ABL flows, the model coefficients are deduced from phenomenological theories of turbulence (Lilly 1967; Antonopoulos-Domis 1981; Mason 1994) and also from models for the effect of stratification and shear on the turbulence (Mason & Thomson 1992; Sullivan *et al.* 1994; Redelsperger *et al.* 2001; Kleissl *et al.* 2003; Sullivan *et al.* 2003). Hence, in simulations, the model coefficients are computed based on predetermined expressions that relate the model coefficients to flow parameters such as the Richardson number, the Obukhov length, and the ratio of filter scale to distance to the ground (Kleissl *et al.* 2006).

A major advancement in subfilter modeling for LES came with the introduction of dynamic procedures to determine the appropriate local value of the model coefficients without any ad-hoc tuning (Germano *et al.* 1991; Moin *et al.* 1991). In this approach, the model coefficients are obtained by comparing the eddy dissipation at different scales. Although the dynamic model removes the need for prescribed stability and shear dependence, it assumes that the model coefficients are scale invariant. The assumption of scale invariance in the standard dynamic model was relaxed through the development of scale-dependent dynamic models (Meneveau & Katz 2000; Porté-Agel *et al.* 2000; Porté-Agel 2004). It has been shown that the dynamic model gives better subfilter dissipation characteristics with respect to the traditional model, especially in the surface layer where the relative contribution of the subfilter scales to the overall turbulent fluxes is very large (Bou-Zeid *et al.* 2005; Kleissl *et al.* 2006; Stoll & Porté-Agel 2008; Khani & Waite 2015). However, a disadvantage of this approach lies in its increased computational complexity compared to the traditional model and in the need for averaging and clipping to attain numerical stability (Ghosal *et al.* 1995; Meneveau *et al.* 1996; Vreman *et al.* 1997).

An alternative approach to defining the subfilter turbulent fluxes is provided by minimum-dissipation models. This new category of subfilter models provides the minimum eddy dissipation required to dissipate the energy of the subfilter scales. The first minimum-dissipation eddy-viscosity model is the QR model, which is based on the invariants of the resolved strain-rate tensor and was developed for isotropic grids (Verstappen *et al.* 2010). Later, Rozema *et al.* (2015) generalized the properties of this model to anisotropic grids by introducing an anisotropic minimum-dissipation (AMD) model. Recently, Abkar *et al.* (2016) extended the AMD approach to modeling the subfilter scalar flux. Of its many desirable practical and theoretical properties, the AMD model has low computational complexity, switches off in laminar and transitional flows, and is consistent with the exact subfilter stress tensor and scalar flux on both isotropic and anisotropic grids. This model has been successfully applied in simulations of decaying grid turbulence, in simulations of a temporal mixing layer and turbulent channel flow (Rozema *et al.* 2015), and in simulations of a high-Reynolds-number rough-wall boundary layer with a constant surface scalar flux (Abkar *et al.* 2016). However, previous studies using minimum-dissipation models ignored the effect of buoyancy.

In this study, the AMD model is generalized to include the effect of buoyancy and is tested by simulating a thermally stratified ABL. The derivation of the AMD model is provided in Section 2. The LES framework and the numerical setup are described in Section 3. LES results are presented in Section 4, and conclusions are provided in Section 5.

2. Anisotropic minimum-dissipation model

A minimum-dissipation model imposes that the energy of the subfilter scales of the LES solution does not increase

$$\partial_t \int_{\Omega_b} \frac{1}{2}\tilde{u}_i'\tilde{u}_i' dx \leq 0, \qquad \tilde{u}_i' = \tilde{u}_i - \frac{1}{|\Omega_b|}\int_{\Omega_b} \tilde{u}_i dx,$$

$$\partial_t \int_{\Omega_b} \frac{1}{2}\tilde{\theta}'\tilde{\theta}' dx \leq 0, \qquad \tilde{\theta}' = \tilde{\theta} - \frac{1}{|\Omega_b|}\int_{\Omega_b} \tilde{\theta} dx, \tag{2.1}$$

where $\tilde{u}_i'$ and $\tilde{\theta}'$ are the subfilter scales corresponding to the filter box with domain Ω_b applied to the LES solution, and $x \in \Omega_b$. For a rectangular filter box Ω_b, with dimensions of δ_1, δ_2 and δ_3, an upper bound for the subfilter energy can be obtained using the Poincaré inequality. There are different formulations of the Poincaré inequality, otherwise known as the Poincaré-Wirtinger inequality

$$\int_{\Omega_b} \frac{1}{2}\tilde{u}_i'\tilde{u}_i' dx \leq \int_{\Omega_b} \frac{1}{2}(\hat{\partial}_i\tilde{u}_j)(\hat{\partial}_i\tilde{u}_j) dx,$$

$$\int_{\Omega_b} \frac{1}{2}\tilde{\theta}'\tilde{\theta}' dx \leq \int_{\Omega_b} \frac{1}{2}(\hat{\partial}_i\tilde{\theta})(\hat{\partial}_i\tilde{\theta}) dx, \tag{2.2}$$

where $\hat{\partial}_i = C_i\delta_i\partial_i$ (for $i = 1, 2, 3$) is the scaled gradient operator; C_i is a modified Poincaré constant; and $(\hat{\partial}_i\tilde{u}_j)(\hat{\partial}_i\tilde{u}_j)/2$ and $(\hat{\partial}_i\tilde{\theta})(\hat{\partial}_i\tilde{\theta})/2$ are the scaled velocity and temperature gradient intensity, respectively. The modified Poincaré constant is independent of the size of the filter box, and its magnitude depends only on the accuracy of the discretization method (i.e., order of accuracy) for each direction (Rozema *et al.* 2015; Abkar *et al.* 2016).

The Poincaré inequality indicates that the energy of the subfilter scales can be confined by imposing a bound on the scaled velocity and potential temperature gradient intensity. If the eddy viscosity, the eddy diffusivity, and the filter widths are assumed to be constant in the filter box Ω_b, then the evolution equations for the scaled velocity and potential temperature gradient intensity can be expressed as

$$\partial_t\left(\frac{1}{2}(\hat{\partial}_i\tilde{u}_j)(\hat{\partial}_i\tilde{u}_j)\right) = -(\hat{\partial}_k\tilde{u}_i)(\hat{\partial}_k\tilde{u}_j)\tilde{S}_{ij} - (\nu+\nu_e)\hat{\partial}_k(\partial_i\tilde{u}_j)\hat{\partial}_k(\partial_i\tilde{u}_j) + \delta_{i3}\beta(\hat{\partial}_k\tilde{u}_i)\hat{\partial}_k(\tilde{\theta} - \langle\tilde{\theta}\rangle) + \partial_i f_i,$$

$$\partial_t\left(\frac{1}{2}(\hat{\partial}_i\tilde{\theta})(\hat{\partial}_i\tilde{\theta})\right) = -(\hat{\partial}_k\tilde{u}_i)(\hat{\partial}_k\tilde{\theta})\partial_i\tilde{\theta} - (D+D_e)\hat{\partial}_k(\partial_i\tilde{\theta})\hat{\partial}_k(\partial_i\tilde{\theta}) + \partial_i g_i, \tag{2.3}$$

where f_i and g_i are the fluxes of velocity and temperature gradient intensity, respectively. Upon spatial integration over the filter box Ω_b, the divergence terms, $\partial_i f_i$ and $\partial_i g_i$, can be rewritten to a boundary integral. Boundary integrals express transport of the velocity and temperature gradient intensity instead of production or dissipation, and they are therefore ignored in the derivation of the AMD model. Note that the Coriolis force has no contribution in the above equations.

The dissipation at the scale of a filter box can be approximated by the application of the Poincaré inequality

$$\int_{\Omega_b} (\partial_i\tilde{u}_j)(\partial_i\tilde{u}_j) \leq \int_{\Omega_b} \hat{\partial}_k(\partial_i\tilde{u}_j)\hat{\partial}_k(\partial_i\tilde{u}_j) dx,$$

$$\int_{\Omega_b} (\partial_i \tilde{\theta})(\partial_i \tilde{\theta}) \leq \int_{\Omega_b} \hat{\partial}_k(\partial_i \tilde{\theta})\hat{\partial}_k(\partial_i \tilde{\theta})dx. \tag{2.4}$$

As a result, the eddy-viscosity and the eddy-diffusivity models give sufficient eddy dissipation to cancel the production of scaled velocity and potential temperature gradient energy, respectively, if the following inequalities hold

$$\int_{\Omega_b} -(\hat{\partial}_k \tilde{u}_i)(\hat{\partial}_k \tilde{u}_j)\tilde{S}_{ij}dx + \int_{\Omega_b} \delta_{i3}\beta(\hat{\partial}_k \tilde{u}_i)\hat{\partial}_k(\tilde{\theta} - \langle\tilde{\theta}\rangle)dx \leq \nu_e \int_{\Omega_b} (\partial_i \tilde{u}_j)(\partial_i \tilde{u}_j)dx,$$

$$\int_{\Omega_b} -(\hat{\partial}_k \tilde{u}_i)(\hat{\partial}_k \tilde{\theta})\partial_i \tilde{\theta}dx \leq D_e \int_{\Omega_b} (\partial_i \tilde{\theta})(\partial_i \tilde{\theta})dx. \tag{2.5}$$

Taking the minimum eddy dissipation that satisfies these conditions gives

$$\nu_e = \frac{\int_{\Omega_b} -(\hat{\partial}_k \tilde{u}_i)(\hat{\partial}_k \tilde{u}_j)\tilde{S}_{ij}dx + \int_{\Omega_b} \delta_{i3}\beta(\hat{\partial}_k \tilde{u}_i)\hat{\partial}_k(\tilde{\theta} - \langle\tilde{\theta}\rangle)dx}{\int_{\Omega_b} (\partial_l \tilde{u}_m)(\partial_l \tilde{u}_m)dx},$$

$$D_e = \frac{\int_{\Omega_b} -(\hat{\partial}_k \tilde{u}_i)(\hat{\partial}_k \tilde{\theta})\partial_i \tilde{\theta}dx}{\int_{\Omega_b} (\partial_l \tilde{\theta})(\partial_l \tilde{\theta})dx}. \tag{2.6}$$

By approximating the integrals over the filter box using the mid-point rule for integration, the AMD eddy-viscosity and eddy-diffusivity models can be written as

$$\nu_e = \frac{-(\hat{\partial}_k \tilde{u}_i)(\hat{\partial}_k \tilde{u}_j)\tilde{S}_{ij} + \delta_{i3}\beta(\hat{\partial}_k \tilde{u}_i)\hat{\partial}_k(\tilde{\theta} - \langle\tilde{\theta}\rangle)}{(\partial_l \tilde{u}_m)(\partial_l \tilde{u}_m)},$$

$$D_e = \frac{-(\hat{\partial}_k \tilde{u}_i)(\hat{\partial}_k \tilde{\theta})\partial_i \tilde{\theta}}{(\partial_l \tilde{\theta})(\partial_l \tilde{\theta})}. \tag{2.7}$$

The AMD model is consistent with the exact subfilter stress tensor and heat flux on both isotropic and anisotropic grids. Taylor expansion of the subfilter turbulent fluxes gives

$$\begin{aligned} \tau_{ij} &= \widetilde{u_i u_j} - \tilde{u}_i \tilde{u}_j = (\hat{\partial}_k \tilde{u}_i)(\hat{\partial}_k \tilde{u}_j) + \mathcal{O}(\delta x_i^4), \\ q_i &= \widetilde{u_i \theta} - \tilde{u}_i \tilde{\theta} = (\hat{\partial}_k \tilde{u}_i)(\hat{\partial}_k \tilde{\theta}) + \mathcal{O}(\delta x_i^4). \end{aligned} \tag{2.8}$$

The eddy dissipation of the exact subfilter turbulent fluxes is

$$\begin{aligned} &- \tau_{ij}\tilde{S}_{ij} + \delta_{i3}\beta(\widetilde{u_i(\theta - \langle\theta\rangle)} - \tilde{u}_i(\tilde{\theta} - \langle\tilde{\theta}\rangle)) = \\ &\quad - (\hat{\partial}_k \tilde{u}_i)(\hat{\partial}_k \tilde{u}_j)\tilde{S}_{ij} + \delta_{i3}\beta(\hat{\partial}_k \tilde{u}_i)\hat{\partial}_k(\tilde{\theta} - \langle\tilde{\theta}\rangle) + \mathcal{O}(\delta x_i^4), \end{aligned}$$

$$-q_i \partial_i \tilde{\theta} = -(\hat{\partial}_k \tilde{u}_i)(\hat{\partial}_k \tilde{\theta})\partial_i \tilde{\theta} + \mathcal{O}(\delta x_i^4). \tag{2.9}$$

As shown in these equations, the leading-order terms of these expansions are proportional to the terms in the numerator of Eq. (2.7).

In practical applications of the AMD model, the size of the filter box is set equal to a grid cell ($\delta_i = \Delta_i$), and the corresponding Poincaré constant is chosen according to the accuracy of the discretization method for each direction. In particular, for a rectangular filter box, the Poincaré constant is $1/\sqrt{12}$ for a spectral method, and it is equal to $1/\sqrt{3}$ for a second-order accurate scheme (Verstappen *et al.* 2010, 2014). In addition, to ensure numerical stability, the eddy viscosity and eddy diffusivity are restricted to having non-negative values to avoid local kinetic energy transfer from unresolved to resolved scales (Rozema *et al.* 2015; Abkar *et al.* 2016). Note that the computational complexity

of the AMD model is comparable to the computational complexity of the traditional Smagorinsky model. However, unlike the traditional model, the AMD model switches off in the laminar and transitional flows, and it does not need any ad-hoc stability and shear corrections.

3. Numerical simulation

Eq. 1.1 is solved numerically by discretizing the computational domain into N_x, N_y, and N_z uniformly spaced grid points with the resolution of Δ_x, Δ_y, and Δ_z in the streamwise, spanwise, and wall-normal directions, respectively. In horizontal directions, pseudo-spectral discretization and periodic boundary conditions are used, while the wall-normal direction is discretized with a second-order accurate method. Hence, in the AMD model, we adopt $C_x = C_y = 1/\sqrt{12}$ and $C_z = 1/\sqrt{3}$ for the modified Poincaré constant. The time advancement is based on a second-order accurate Adams-Bashforth scheme. Full dealiasing of the nonlinear terms is obtained by padding and truncation according to the 3/2 rule (Canuto *et al.* 1988). The upper boundary condition for the momentum conservation equations consists of a stress-free condition and zero vertical velocity. The temperature gradient at the top of the domain is set to a constant lapse rate Γ, which is prescribed in the initial conditions. At the bottom surface, the instantaneous wall stress and heat flux are related to the velocity and potential temperature, respectively, at the first vertical node through the application of the Monin-Obukhov similarity theory (Moeng 1984)

$$\tau_{i3}|_w = -u_*^2 \frac{\tilde{u}_i}{\tilde{u}_r} = -\left[\frac{\tilde{u}_r \kappa}{\ln(z/z_o) - \Psi_M}\right]^2 \frac{\tilde{u}_i}{\tilde{u}_r}, \qquad q_3|_w = \frac{u_* \kappa(\theta_s - \tilde{\theta})}{\ln(z/z_{ot}) - \Psi_H}, \tag{3.1}$$

where $\tau_{i3}|_w$ and $q_3|_w$ are the instantaneous local wall stress and heat flux, respectively; u_* is the friction velocity; z_o and z_{ot} are the surface roughness for momentum and potential temperature, respectively; κ is the von Kármán constant; $\tilde{u}_r$ is the local filtered horizontal velocity at the first level $z = \Delta_z/2$; and θ_s is the surface (ground level) potential temperature. Ψ_M and Ψ_H are the surface-layer stability corrections for momentum and heat, respectively, and are defined as (Businger *et al.* 1971; Stull 1988)

$$\Psi_M = \begin{cases} -4.7\ z/L & \text{for } z/L \geq 0, \\ 2\ln[\tfrac{1}{2}(1+\zeta)] + \ln[\tfrac{1}{2}(1+\zeta^2)] - 2\tan^{-1}[\zeta] + \pi/2 & \text{for } z/L < 0, \end{cases}$$

$$\Psi_H = \begin{cases} -7.8\ z/L & \text{for } z/L \geq 0, \\ 2\ln[\tfrac{1}{2}(1+\zeta^2)] & \text{for } z/L < 0, \end{cases} \tag{3.2}$$

where $L = -(u_*^3 \theta_0)/(\kappa g q_3|_w)$ is the local Obukhov length, and $\zeta = (1 - 15\ z/L)^{1/4}$.

4. Results

In this section, the performance of the AMD model is tested in a simulation of a thermally stratified ABL. In this regard, a convective boundary layer similar to the one used by Moeng & Sullivan (1994) is considered. This case represents a buoyancy-dominated flow with a relatively small shear effect. The boundary layer is driven by an imposed, uniform geostrophic wind of 10 m/s. The surface heat flux is set to 0.24 K m/s. The surface roughness length for momentum and heat is set to 0.16 m. The Coriolis parameter is $f_c = 1 \times 10^4$ rad/s. The domain size is 5 km $\times$ 5 km $\times$ 2 km. The simulations

Grid points	z_i [m]	L [m]	u_* [m/s]	w_* [m/s]
$48 \times 48 \times 48$	1021	−59.6	0.570	2.00
$72 \times 72 \times 72$	1014	−58.9	0.568	1.99
$96 \times 96 \times 96$	1032	−59.2	0.569	2.00

TABLE 1. Basic characteristics of the simulated convective boundary layer.

are initialized with a constant streamwise velocity of 10 m/s and zero velocity for the spanwise and vertical components. The initial potential temperature profile is 300 K up to 937 m. It increases by a total of 8 K across 126 m, and then increases with a lapse rate of 3 K/km. The reference potential temperature is $\theta_0 = 301.78$ K. In the simulations, three different spatial resolutions of $48 \times 48 \times 48$, $72 \times 72 \times 72$ and $96 \times 96 \times 96$ are used to assess the grid-resolution sensitivity of the simulation results. Table 1 provides a summary of the mean simulated results, including the boundary-layer height z_i (i.e., the height where the buoyancy flux is minimum (Sullivan *et al.* 1994)), the Obukhov length L, the friction velocity u_*, and the convective velocity $\left(w_* = (g/\theta_0)q_3|_w z_i)^{1/3}\right)$. Note that the simulations are run for 9000 seconds, which is about 17 large-eddy turnover times ($\tau_* = z_i/w_*$), and the statistics are computed during the last five large-eddy turnover times. From this table, it is evident that the simulated (bulk) boundary-layer parameters are quite insensitive to the grid resolution.

Figure 1(a,b) shows the vertical profiles of the mean winds and potential temperature, respectively. The well-mixed layer over the interior of the boundary layer is clearly observed, which indicates the effectiveness of turbulent mixing in the convective boundary layers (Moeng & Sullivan 1994). The nondimensional gradients of shear and potential temperature are also plotted in Figure 2(a,b), respectively, and compared with the empirical formulations proposed by Businger *et al.* (1971)

$$\Phi_M = (1 - 15\ z/L)^{-1/4}, \quad \Phi_H = 0.74(1 - 9\ z/L)^{-1/2}. \tag{4.1}$$

As can be seen, the agreement between the LES results and the well-established empirical correlations is quite good. In addition, the results show very little sensitivity to grid resolution.

The vertical distributions of the total (resolved plus subfilter) momentum and buoyancy fluxes are shown in Figure 3(a,b), respectively. As can be seen, the magnitude of the turbulent fluxes decreases linearly with height, which can serve as confirmation of stationarity. Similar behavior has been reported by Nieuwstadt *et al.* (1993) and Moeng & Sullivan (1994) in simulations of buoyancy-driven ABL flows. The variances of the horizontal and vertical velocity fluctuations as a function of z/z_i are presented in Figure 4(a,b), respectively. Some observations obtained from atmospheric field experiments (Lenschow *et al.* 1980) are also plotted for comparison. It is observed that the LES results agree very well with the measurement data, and they show very weak dependence on the spatial resolutions.

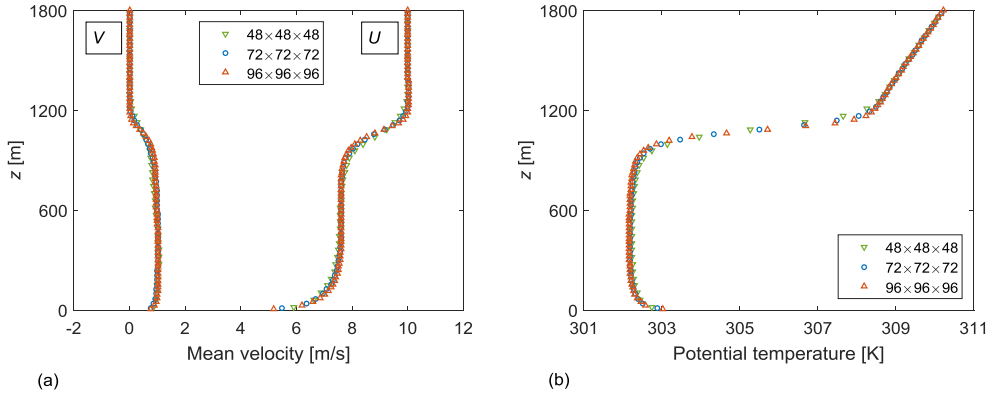

FIGURE 1. Vertical profiles of the mean (a) streamwise (U) and spanwise (V) velocities and (b) potential temperature.

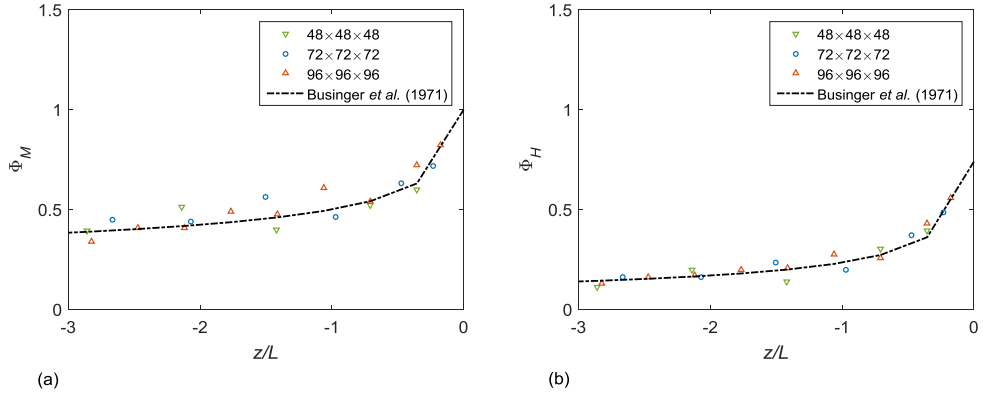

FIGURE 2. Nondimensional gradients of (a) velocity and (b) temperature as a function of the stability parameter z/L. The dash-dotted lines correspond to the formulations proposed by Businger *et al.* (1971).

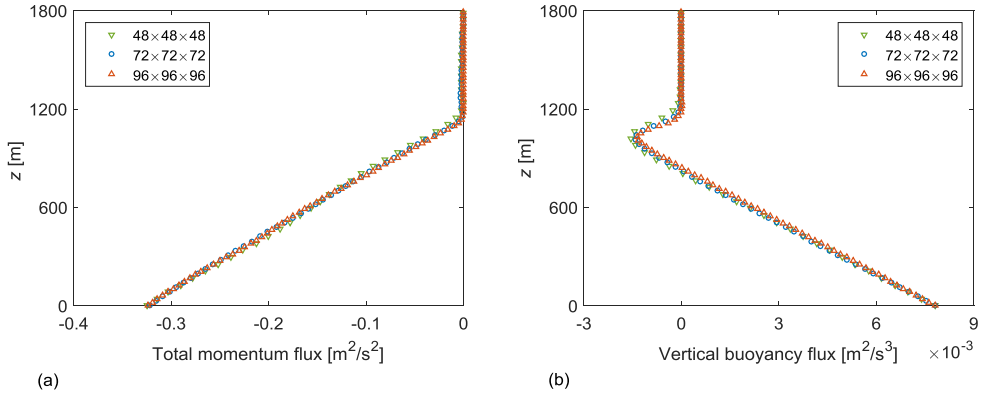

FIGURE 3. Vertical profiles of the (a) total momentum and (b) buoyancy fluxes.

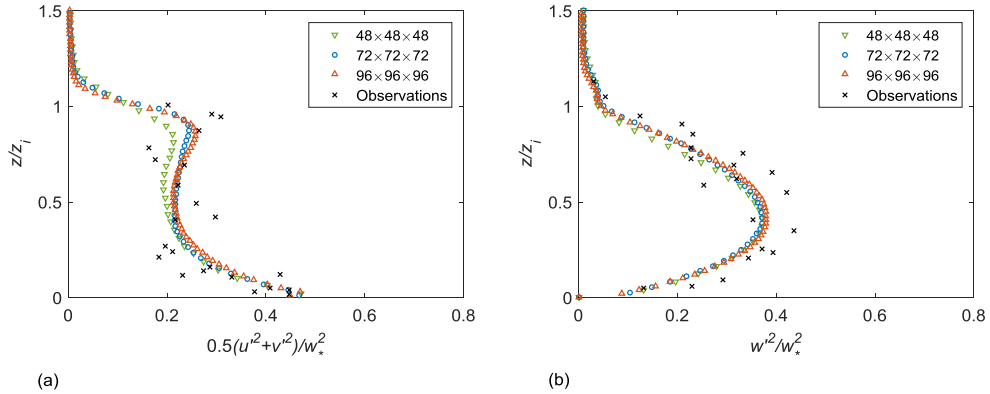

FIGURE 4. Vertical profiles of the normalized (a) horizontal and (b) vertical velocity variances.

5. Conclusion

Minimum-dissipation models are a new class of subfilter models that give the minimum eddy dissipation required to dissipate the energy of subfilter scales. In this study, a generalized form of the recently developed minimum-dissipation model (Abkar *et al.* 2016) was proposed to include the effect of buoyancy, in addition to shear, on the production and suppression of turbulence. The proposed model has many desirable properties. Specifically, it appropriately switches off in laminar and transitional flows, has low computational complexity, and is consistent with the exact subfilter turbulent fluxes. The performance of the proposed model was tested in simulations of a convective boundary layer. The simulation results show very good agreement with the well-established empirical correlations, theoretical predictions, and field observations. In particular, the proposed model is capable of accurately reproducing the expected surface-layer similarity profiles for both velocity and potential temperature. This is particularity important since, the relative contribution of the subfilter scales to the overall turbulent fluxes is very large in the surface layer, and the gradients are also stronger in that region. In addition, the simulation results show very weak grid-resolution dependence, which indicates the robustness of the proposed model in the simulation of ABLs, even with relatively coarse resolutions.

Acknowledgments

The authors acknowledge support from NASA, Grant # NNX15AU93A. M. A. is grateful to the Swiss National Science Foundation for its postdoctoral fellowship support. The authors also thank Dr. Curtis Hamman for his useful comments on the manuscript.

REFERENCES

ABKAR, M., BAE, H. & MOIN, P. 2016 Minimum-dissipation scalar transport model for large-eddy simulation of turbulent flows. *Phys. Rev. Fluids* **1**, 041701.

ANTONOPOULOS-DOMIS, M. 1981 Large-eddy simulation of a passive scalar in isotropic turbulence. *J. Fluid Mech.* **104**, 55–79.

BEARE, R. J., MACVEAN, M. K., HOLTSLAG, A. A. M., CUXART, J., ESAU, I., GOLAZ, J.-C., JIMENEZ, M. A., KHAIROUTDINOV, M., KOSOVIC, B., LEWELLEN,

D., Lund, T. S., Lundquist, J. K., McCabe, A., Moene, A. F., Noh, Y., Raasch, S. & Sullivan, P. 2006 An intercomparison of large-eddy simulations of the stable boundary layer. *Bound.-Lay. Meteorol.* **118**, 247–272.

Bou-Zeid, E., Meneveau, C. & Parlange, M. 2005 A scale-dependent Lagrangian dynamic model for large eddy simulation of complex turbulent flows. *Phys. Fluids.* **17**, 025105.

Businger, J. A., Wyngaard, J. C., Izumi, Y. & Bradley, E. F. 1971 Flux-profile relationships in the atmospheric surface layer. *J. Atmos. Sci.* **28**, 181–189.

Canuto, C., Hussaini, M., Quarteroni, A. & Zang, T. 1988 *Spectral Methods in Fluid Dynamics*. Springer.

Deardorff, J. W. 1974 Three-dimensional numerical study of the height and mean structure of a heated planetary boundary layer. *Bound.-Lay. Meteorol.* **7**, 81–106.

Germano, M., Piomelli, U., Moin, P. & Cabot, W. 1991 A dynamic subgrid-scale eddy viscosity model. *Phys. Fluids* **3**, 1760–1765.

Ghosal, S., Lund, T. S., Moin, P. & Akselvoll, K. 1995 A dynamic localization model for large-eddy simulation of turbulent flows. *J. Fluid Mech.* **286**, 229–255.

Khani, S. & Waite, M. L. 2015 Large eddy simulations of stratified turbulence: the dynamic Smagorinsky model. *J. Fluid Mech.* **773**, 327–344.

Kleissl, J., Kumar, V., Meneveau, C. & Parlange, M. B. 2006 Numerical study of dynamic Smagorinsky models in large-eddy simulation of the atmospheric boundary layer: Validation in stable and unstable conditions. *Water Resour. Res.* **42**, W06D10.

Kleissl, J., Meneveau, C. & Parlange, M. B. 2003 On the magnitude and variability of subgrid-scale eddy-diffusion coefficients in the atmospheric surface layer. *J. Atmos. Sci.* **60**, 2372–2388.

Kosovic, B. 1997 Subgrid-scale modelling for the large-eddy simulation of high-Reynolds-number boundary layers. *J. Fluid Mech.* **336**, 151–182.

Lenschow, D., Wyngaard, J. C. & Pennell, W. T. 1980 Mean-field and second-moment budgets in a baroclinic, convective boundary layer. *J. Atmos. Sci.* **37**, 1313–1326.

Lilly, D. K. 1967 The representation of small-scale turbulence in numerical simulation experiments. In *Proceedings of the IBM Scientific Computing Symposium on Environmental Sciences*, p. 167. Yorktown Heights, NY.

Mason, P. J. 1994 Large-eddy simulation: A critical review of the technique. *Q. J. Roy. Meteor. Soc.,* **120**, 1–26.

Mason, P. J. & Thomson, D. J. 1992 Stochastic backscatter in large-eddy simulations of boundary layers. *J. Fluid Mech.* **242**, 51–78.

Meneveau, C. & Katz, J. 2000 Scale-invariance and turbulence models for large-eddy simulation. *Annu. Rev. Fluid Mech.* **32**, 1–32.

Meneveau, C., Lund, T. S. & Cabot, W. H. 1996 A Lagrangian dynamic subgrid-scale model of turbulence. *J. Fluid Mech.* **319**, 353–385.

Moeng, C. 1984 A large-eddy simulation model for the study of planetary boundary-layer turbulence. *J. Atmos. Sci.* **46**, 2311–2330.

Moeng, C.-H. & Sullivan, P. P. 1994 A comparison of shear- and buoyancy-driven planetary boundary layer flows. *J. Atmos. Sci.* **51**, 999–1022.

Moin, P., Squires, K. D. & Lee, S. 1991 A dynamic subgrid-scale model for compressible turbulence and scalar transport. *Phys. Fluids* **3**, 2746.

Nieuwstadt, F. T., Mason, P. J., Moeng, C.-H. & Schumann, U. 1993 Large-

eddy simulation of the convective boundary layer: A comparison of four computer codes. In *Turbulent Shear Flows 8: Selected Papers from the Eighth International Symposium on Turbulent Shear Flows,* F. Durst *et al.* (Eds.), Springer-Verlag, 343–367.

Porté-Agel, F. 2004 A scale-dependent dynamic model for scalar transport in large-eddy simulations of the atmospheric boundary layer. *Bound.-Lay. Meteorol.* **112**, 81–105.

Porté-Agel, F., Meneveau, C. & Parlange, M. B. 2000 A scale-dependent dynamic model for large-eddy simulation: application to a neutral atmospheric boundary layer. *J. Fluid Mech.* **415**, 261–284.

Redelsperger, J.-L., Mahé, F. & Carlotti, P. 2001 A simple and general subgrid model suitable both for surface layer and free-stream turbulence. *Bound.-Lay. Meteorol.* **101**, 375–408.

Rozema, W., Bae, H. J., Moin, P. & Verstappen, R. 2015 Minimum-dissipation models for large-eddy simulation. *Phys. Fluids* **27**, 085107.

Smagorinsky, J. 1963 General circulation experiments with the primitive equations. *Mon. Weather Rev.* **91**, 99–164.

Stoll, R. & Porté-Agel, F. 2008 Large-eddy simulation of the stable atmospheric boundary layer using dynamic models with different averaging schemes. *Bound.-Lay. Meteorol.* **126**, 1–28.

Stull, R. 1988 *An introduction to boundary-layer meteorology*. Kluwer Academic Publishers, Dordrecht.

Sullivan, P. P., Horst, T. W., Lenschow, D. H., Moeng, C.-H. & Weil, J. C. 2003 Structure of subfilter-scale fluxes in the atmospheric surface layer with application to large-eddy simulation modelling. *J. Fluid Mech.* **482**, 101–139.

Sullivan, P. P., McWilliams, J. C. & Moeng, C.-H. 1994 A subgrid-scale model for large-eddy simulation of planetary boundary-layer flows. *Bound.-Lay. Meteorol.* **71**, 247–276.

Sullivan, P. P. & Patton, E. G. 2011 The effect of mesh resolution on convective boundary layer statistics and structures generated by large-eddy simulation. *J. Atmos. Sci.* **68**, 2395–2415.

Verstappen, R., Bose, S., Lee, J., Choi, H. & Moin, P. 2010 A dynamic eddy-viscosity model based on the invariants of the rate-of-strain. *Proceeding of the Summer Program*, Center for Turbulence Research, Stanford University, pp. 183–192.

Verstappen, R., Rozema, W. & Bae, H. 2014 Numerical scale separation in large-eddy simulation. *Proceeding of the Summer Program*, Center for Turbulence Research, Stanford University, pp. 417–426.

Vreman, B., Geurts, B. & Kuerten, H. 1997 Large-eddy simulation of the turbulent mixing layer. *J. Fluid Mech.* **339**, 357–390.

Zhou, B. & Chow, F. K. 2011 Large-eddy simulation of the stable boundary layer with explicit filtering and reconstruction turbulence modeling. *J. Atmos. Sci.* **68**, 2142–2155.